

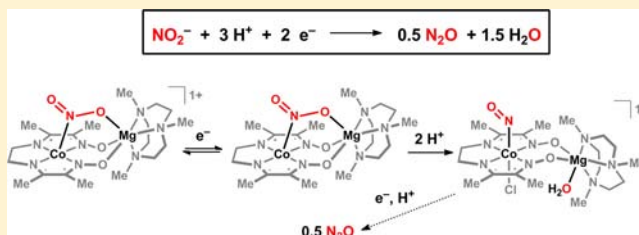
Selective Nitrite Reduction at Heterobimetallic CoMg Complexes

Christopher Uyeda and Jonas C. Peters*

Division of Chemistry and Chemical Engineering, California Institute of Technology, Pasadena, California 91125, United States

S Supporting Information

ABSTRACT: Heme-containing nitrite reductases bind and activate nitrite by a mechanism that is proposed to involve interactions with Brønsted acidic residues in the secondary coordination sphere. To model this functionality using synthetic platforms that incorporate a Lewis acidic site, heterobimetallic CoMg complexes supported by diimine-dioxime ligands are described. The neutral $(\mu\text{-NO}_2)\text{CoMg}$ species **3** is synthesized from the $[(\mu\text{-OAc})(\text{Br})\text{CoMg}]^+$ complex **1** by a sequence of one-electron reduction and ligand substitution reactions. Data are presented for a redox series of nitrite adducts, featuring a conserved $\mu\text{-}(\eta^1\text{-N}:\eta^1\text{-O})\text{-NO}_2$ motif, derived from this synthon. Conditions are identified for the proton-induced N–O bond heterolysis of bound NO_2^- in the most reduced member of this series, affording the $[(\text{NO})(\text{Cl})\text{CoMg}(\text{H}_2\text{O})]^+$ complex **6**. Reduction of this complex followed by protonation leads to the evolution of free N_2O . On the basis of these stoichiometric reactivity studies, the competence of complex **1** as a NO_2^- reduction catalyst is evaluated using electrochemical methods. In bulk electrolysis experiments, conducted at -1.2 V vs SCE using Et_3NHCl as a proton source, N_2O is produced selectively without the competing formation of NH_3 , NH_2OH , or H_2 .



INTRODUCTION

Substrate selectivity has emerged as one of the principle challenges associated with the development of efficient catalysts for the multielectron reduction of small molecules such as NO_2^- , CO_2 , and N_2 . For many systems that operate under acidic conditions, protonation of the catalyst in its reduced state can often compete with substrate coordination and lead to the undesired evolution of H_2 .^{1–3}

Secondary coordination sphere interactions with Brønsted or Lewis acids have been implicated in several metalloenzyme-mediated small-molecule activation processes as a means of promoting substrate binding.⁴ For example, the nitric oxide-forming cytochrome *cd*₁ nitrite reductase has been crystallographically characterized with a heme $(\eta^1\text{-NO}_2)\text{Fe}^{\text{II}}$ unit in which an oxygen atom of the nitrite anion is hydrogen-bonded to a nearby histidine residue.^{5,6} This hydrogen bond plays an important role in stabilizing the enzyme–substrate complex: the single-point mutant substituting alanine for histidine does not detectably bind NO_2^- and exhibits a 100-fold decrease in turnover frequency.⁷ Recent studies of a related nitrite reductase⁸ have led to the suggestion that the high affinity for nitrite in the reduced form of the enzyme—greater even than in the more Lewis acidic Fe(III) state—can be attributed to the cooperative effect of back-donation from the Fe center and stabilization of the accumulated negative charge on oxygen by hydrogen-bond donors. The combination of these interactions results in a relatively short Fe–N distance and a reduced N–O bond order, facilitating the subsequent heterolysis to form an iron nitrosyl and a molecule of water.⁹

The motivation to gain more detailed mechanistic insight into the cooperativity between a reduced metal center and

acidic functionality has led to the development of synthetic platforms that either incorporate hydrogen-bond donors¹⁰ into the ligand framework or contain non-redox-active Lewis acids.¹¹ Herein, we elaborate on this concept in the context of a heterobimetallic CoMg system that coordinates and reduces the nitrite anion. Our approach exploits diimine-dioximes as binucleating ligands, allowing a Mg^{2+} cation to be placed in proximity to a redox-active transition metal.^{12–14} We hypothesized that the Lewis acidic site would enhance the binding affinity of NO_2^- to a low-valent Co center in analogy to the proposed role of the active-site histidine residues in nitrite reductases.

While reduced Co macrocycle complexes typically react rapidly with acids to evolve H_2 ,¹⁵ they have exhibited little propensity to coordinate anionic ligands, including NO_2^- , in the axial position. By contrast, the heterobimetallic $\text{Co}^{\text{(Me)doen}}\text{Mg}$ platform has afforded an opportunity to characterize NO_2^- adducts in three states of oxidation and to conduct a series of stoichiometric protonation and reduction reactions that ultimately yield free N_2O . On the basis of these results, conditions have been identified for the electrocatalytic conversion of NO_2^- to N_2O without competing formation of NH_3 , NH_2OH , or H_2 . Synthetic nitrite reduction catalysts that produce minimal amounts of ammonia have attracted interest for their potential utility in denitrification processes.¹⁶

Received: May 29, 2013

Published: July 18, 2013

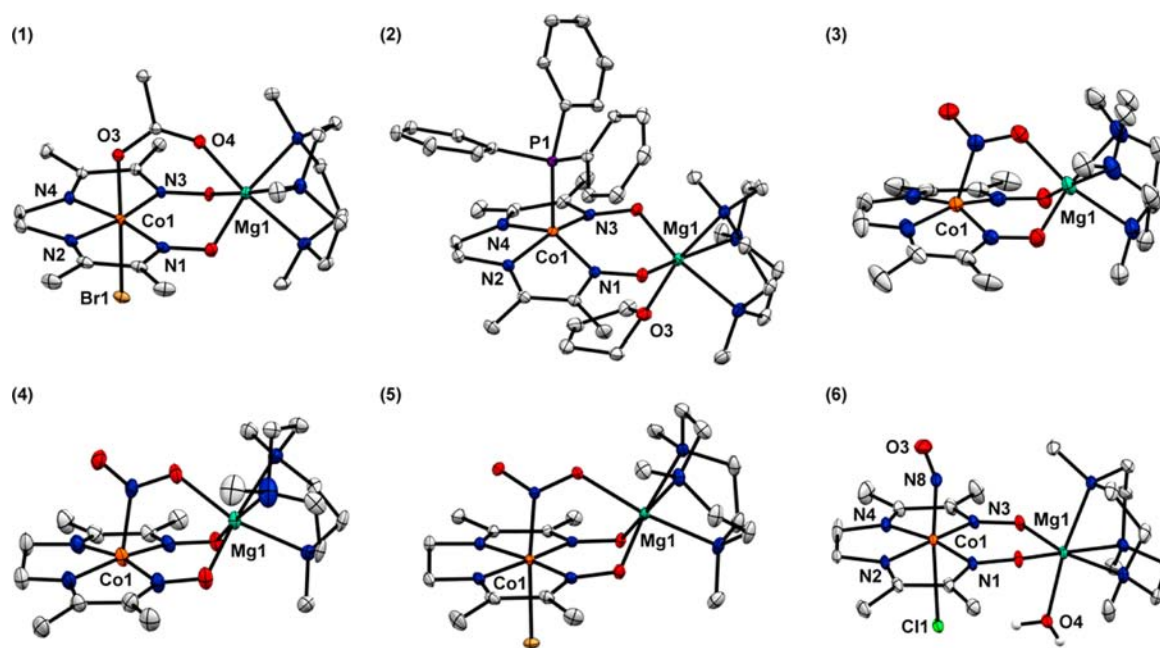


Figure 1. Solid-state structures of 1–6 (thermal ellipsoids at 50% probability). Noncoordinated solvent molecules, counteranions, and hydrogen atoms bound to carbon are excluded for clarity. Selected bond distances (Å) for 1: Co1–N1, 1.9121(8); Co1–N2, 1.872(1); Co1–N3, 1.9179(8); Co1–N4, 1.8621(9); Co1–O3, 1.9303(8); Co1–Br1, 2.3759(2); Mg1–O4, 2.0078(9). Selected bond distances (Å) for 2: Co1–N1, 1.8833(5); Co1–N2, 1.8531(7); Co1–N3, 1.8935(6); Co1–N4, 1.8584(6); Co1–P1, 2.2408(2); Mg1–O3, 2.1504(6). Selected bond distances (Å) and angles (deg) for 6: Co1–N1, 1.917(1); Co1–N2, 1.863(2); Co1–N3, 1.906(1); Co1–N4, 1.858(2); Co1–N8, 1.856(1); Co1–Cl1, 2.6210(4); Mg1–O4, 2.062(1); N8–O3, 1.149(2); Co1–N8–O3, 122.1(1).

RESULTS AND DISCUSSION

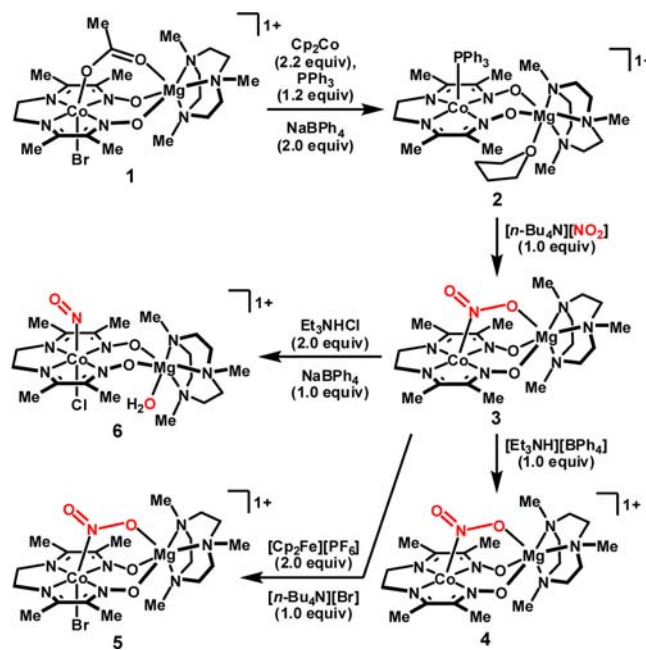
Preparation of a CoMg Complex and Nitrite Binding.

The synthesis of well-defined heterobimetallic complexes remains a frontier area of inorganic synthesis due to the inherent challenges associated with site-selective metalation. One effective approach involves the use of ambidentate ligands, including oximato groups,^{12–14} with differentiated metal-binding sites.

Accordingly, the heterobimetallic $[(\text{Br})(\mu\text{-OAc})\text{Co}(\text{Me}\text{doen})\text{-Mg}]^+$ complex **1** (Figure 1) was prepared from the corresponding monometallic, proton-bridged species $\text{Co}(\text{Me}\text{doenH})\text{Br}_2$ in a reaction with $\text{Mg}(\text{OAc})_2$ and Me_3TACN .^{13c} Association of the nitrite anion with this platform was accomplished in a two-step sequence (Scheme 1). Reduction of complex **1** with 2.2 equiv of Cp_2Co in the presence of PPh_3 and NaBH_4 yielded the dark blue-green, diamagnetic species **2** (³¹P NMR: 43 ppm). Even in the reduced Co(I) state, the Lewis acidity of the pendant Mg center is evident in its affinity for THF, which, likely due to steric constraints, is positioned on the face of the macrocycle opposite the PPh_3 group bound to cobalt (Figure 1).

Facile displacement of coordinated PPh_3 and THF was observed upon treatment of complex **2** with $[\text{n-Bu}_4\text{N}][\text{NO}_2]$, affording the neutral $\mu\text{-}(\eta^1\text{-N}:\eta^1\text{-O})\text{-NO}_2$ species **3** (Figure 1). To accommodate the bridging anion, the Co–Mg distance contracts significantly from 3.7 Å in the PPh_3 adduct **2** to 3.3 Å in complex **3**. Substrate binding in the reduced state is the presumed initial step in nitrite reduction catalytic cycles mediated by cobalt tetraazamacrocyclic complexes;¹⁷ nevertheless, the axial coordination of NO_2^- has not previously been observed in the Co(I) oxidation state, highlighting the role of the Mg^{2+} center in stabilizing this adduct. It is noteworthy in this context that the monometallic, proton-bridged complex

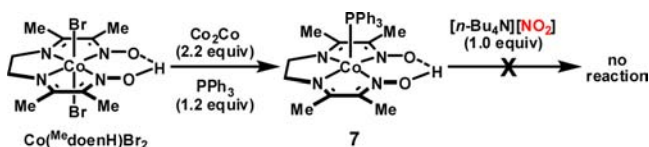
Scheme 1



$(\text{PPh}_3)\text{Co}(\text{Me}\text{doenH})$ (**7**) of the same diimine–dioxime ligand was not observed to undergo ligand substitution in the presence of $[\text{n-Bu}_4\text{N}][\text{NO}_2]$ (Scheme 2).

Significant asymmetry in the nitrite N–O bond lengths is observed in the solid-state structure of complex **3** (Figure 1). IR bands, sensitive to isotopic labeling with ¹⁵ NO_2^- , at 1392 and 1181 cm^{-1} are assigned to N–O stretching vibrations. Complex **3** exhibits a reversible oxidation wave in cyclic voltammetry experiments (MeCN solution, 100 mV/s scan rate) at an E° of

Scheme 2



−0.79 V vs SCE (Figure 2). This potential is approximately 200 mV more positive than is observed for the $\text{Co}^{\text{II/I}}$ redox couple

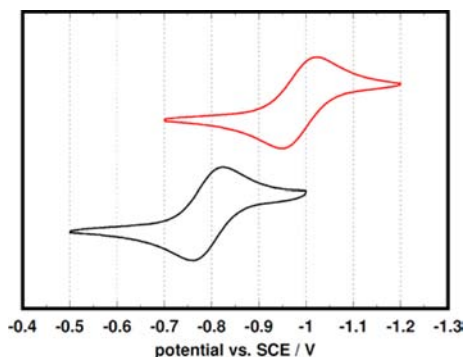


Figure 2. Cyclic voltammograms for complexes **8** (red line, top) and **3** (black line, bottom) isolating the $\text{Co}^{\text{II/I}}$ redox couple (0.5 mM in MeCN, 0.1 M $[\text{n-Bu}_4\text{N}][\text{ClO}_4]$ supporting electrolyte, glassy carbon working electrode, 100 mV/s scan rate).

of the analogous acetate-bridged complex **8** (Figure 3), consistent with a significant stabilization of the reduced state by nitrite relative to acetate.

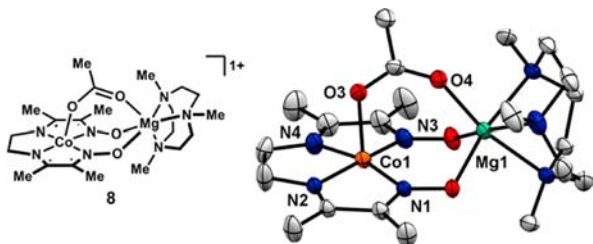


Figure 3. Solid-state structure of **8** (thermal ellipsoids at 50% probability). Noncoordinated solvent molecules, BPh_4^- , and hydrogen atoms bound to carbon are excluded for clarity. Selected bond distances (Å): Co1–N1, 1.903(3); Co1–N2, 1.854(3); Co1–N3, 1.904(3); Co1–N4, 1.858(2); Co1–O3, 2.054(2); Mg1–O4, 2.012(2).

Preparation and Characterization of a Redox Series of $\mu\text{-NO}_2$ Complexes.

The one-electron-oxidized, cationic ($\mu\text{-NO}_2$)CoMg complex **4** is accessed in 76% yield upon treatment of the neutral complex **3** with $[\text{Et}_3\text{NH}][\text{BPh}_4]$. The formation of free H_2 was not observed in this oxidation reaction, suggesting that the ligand may act as a terminal H-atom acceptor, resulting in a less than quantitative yield of complex **4**. In accordance with other low-spin, square-pyramidal Co(II) complexes,¹⁸ the EPR spectrum for this $S = 1/2$ species exhibits rhombic symmetry with a resolved eight-line hyperfine coupling to the ^{59}Co nucleus. The axially coordinated nitrogen donor causes this progression to be further split into either a three-line pattern for the $^{14}\text{NO}_2$ complex or a two-line pattern for the $^{15}\text{NO}_2$ -labeled material (Figure 4b,c respectively). Accordingly, the calculated SOMO (B3LYP/6-31G(d) level of DFT) is of

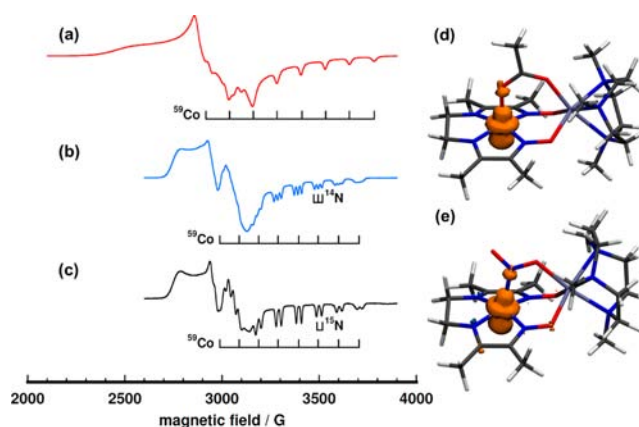


Figure 4. Frozen-solution (77 K) X-band EPR spectra for (a) $[(\mu\text{-OAc})\text{CoMg}]^+$ (**8**), (b) $[(\mu\text{-}^{14}\text{NO}_2)\text{CoMg}]^+$ (**4**), and (c) $[(\mu\text{-}^{15}\text{NO}_2)\text{CoMg}]^+$ (**4**). Calculated spin density plot for (d) $[(\mu\text{-OAc})\text{CoMg}]^+$ and (e) $[(\mu\text{-NO}_2)\text{CoMg}]^+$. Simulated parameters for $[(\mu\text{-OAc})\text{CoMg}]^+$: $g_x = 2.550$, $g_y = 2.270$, $g_z = 2.030$ ($g_{\text{max}} - g_{\text{min}} = 0.52$), $A(\text{Co})_z = 350$ MHz. Simulated parameters for $[(\mu\text{-NO}_2)\text{CoMg}]^+$: $g_x = 2.360$, $g_y = 2.190$, $g_z = 2.032$ ($g_{\text{max}} - g_{\text{min}} = 0.33$), $A(\text{Co})_z = 300$ MHz, $A(\text{N})_z = 60$ MHz. See the Supporting Information for simulated spectra.

d_z^2 parentage, and the spin density (Figure 4e), by Mulliken population analysis, is largely localized on cobalt. In comparison to the analogous cationic ($\mu\text{-OAc})\text{Co}^{\text{II}}$ complex **8** (Figure 4a), the $\mu\text{-NO}_2$ complex exhibits both a smaller ^{59}Co coupling constant and less g anisotropy ($g_{\text{max}} - g_{\text{min}}$), indicative of a decrease in spin density at the metal center.¹⁹

While a second oxidation wave for complex **3** was not observed by cyclic voltammetry up to potentials of +0.5 V vs SCE, a ($\mu\text{-NO}_2$)Co^{III} complex is accessible by reaction with 2 equiv of $[\text{Cp}_2\text{Fe}][\text{PF}_6]$ in the presence of a halide source. The structure of the resulting diamagnetic, orange species **5** was confirmed by XRD to be pseudo-octahedral at cobalt with *trans*-coordinated NO_2 and Br anions (Figure 1).

Access to the nitrite complexes **3**, **4**, and **5** affords an unusual opportunity to compare their solid-state structures as a function of the oxidation state. Key bond distances and angles for each of these $\mu\text{-NO}_2$ complexes are summarized in Table 1. The competing effects of electrostatics and back-bonding in the Co– N_{NO_2} interaction are manifested in the Co– N_{NO_2} bond distance, which is shortest in the most oxidized species (**5**), lengthens in the five-coordinate Co(II) complex (**4**), and is modestly contracted in the most reduced species (**3**). The N– O_{Mg} bond distance of the bound NO_2^- , by contrast, monotonically lengthens upon successive addition of electrons from **5** to **4** to **3**. This decrease in nitrite N–O bond order upon reduction is also observed in the corresponding IR stretching frequencies (Figure 5). These vibrations, assigned on the basis of sensitivity to isotopic labeling with $^{15}\text{NO}_2^-$, span approximately 70 cm^{-1} across the range of oxidation states.

The metrical parameters associated with the diimine–dioxime ligand in the neutral $\mu\text{-NO}_2$ complex **3** reveals characteristics that are indicative of significant ligand-centered reduction: C–N distances are elongated, and the intervening C–C distance is contracted relative to either complex **4** or complex **5**. The magnitude and direction of these changes are similar to those of a recently characterized $S = 1/2$ reduced nickel diimine–dioxime complex that was assigned as a ligand-centered radical bound to Ni(II).^{12,20}

Table 1. Selected Bond Distances (Å) and Angles (deg) from Solid-State Structures

	3 ^a	4	5
N–O _{terminal}	1.228(6), 1.241(9)	1.219(5)	1.224(1)
N–O _{Mg}	1.298(6), 1.307(8)	1.285(7)	1.270(1)
Co–N _{NO₂}	1.987(5), 1.978(7)	2.037(5)	1.909(1)
Co–N _{oxime}	1.890(3), 1.885(3)	1.906(2), 1.910(2)	1.914(1), 1.913(1)
Co–N _{imine}	1.839(4), 1.844(4)	1.854(2), 1.858(2)	1.873(1), 1.863(1)
Mg–O _{NO₂}	2.094(4), 2.098(4)	2.079(3)	2.130(1)
∑N–Co–N	351, 352	358	360
C–N _{oxime}	1.330(5), 1.337(5)	1.318(3), 1.320(3)	1.319(2), 1.315(2)
C–N _{imine}	1.316(6), 1.318(6)	1.289(3), 1.291(3)	1.293(2), 1.286(2)
C _{oxime} –C _{imine}	1.427(6), 1.429(6)	1.463(3), 1.462(3)	1.468(2), 1.473(2)
N–O _{oxime}	1.342(4), 1.343(4)	1.321(2), 1.325(3)	1.312(1), 1.312(1)

^aMetrical parameters are shown for two crystallographically distinct molecules in the asymmetric unit. Each molecule is bisected by a mirror plane.

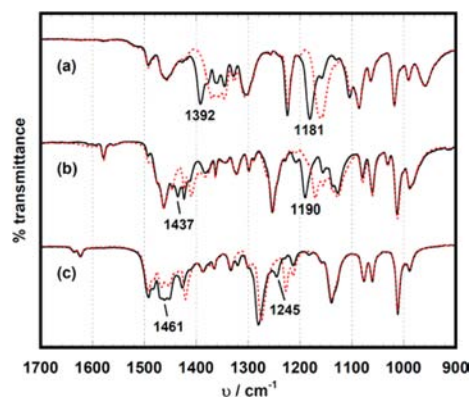


Figure 5. ATR-IR spectra (solid samples) of (a) 3, (b) 4, and (c) 5 prepared with either ¹⁴NO₂[−] (solid, black line) or ¹⁵NO₂[−] (red, dotted line). N–O stretching frequencies for the ¹⁴NO₂[−] compound are indicated.

Additional insight into the electronic structure of complex 3 was obtained from computational models using DFT methods. Its calculated HOMO has both Co d_{z²} character and significant density in the conjugated π-system of the ligand (Figure 6b). Displacement of Co out of the mean N₄ plane, observed both

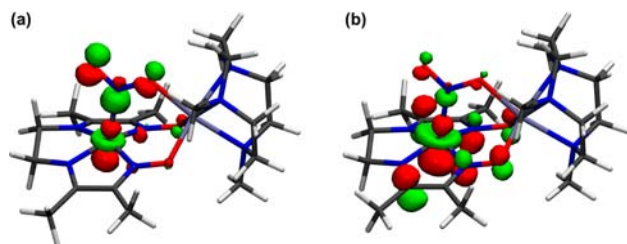


Figure 6. Isosurface representations of the calculated HOMO for the (a) cationic and (b) neutral (μ-NO₂)CoMg complexes at the B3LYP/6-31G(d) level of DFT.

experimentally and computationally, allows for significant overlap of these metal and ligand orbitals. In the cationic complex 4, by comparison, Co is nearly coplanar with the mean N₄ plane, and the SOMO has negligible population on the diimine–dioxime ligand. The ligand geometry is unperturbed relative to that of the Co(III) complex 5 with the exception of moderately elongated oxime N–O distances.

Heterolytic N–O Bond Cleavage Reactivity and Stoichiometric N₂O Production. Because the aforementioned attempted protonation reaction of the neutral μ-NO₂ complex 3 with [Et₃NH][BPh₄][−] resulted instead in its oxidation to the isostructural cation, a broader range of electrophiles was surveyed to identify conditions that effect N–O bond cleavage over competing one-electron redox chemistry. To this end, treatment of complex 3 with excess (TMS)Cl resulted in the formation of a nitrosyl-containing product, readily identified by IR spectroscopy. Hypothesizing the importance of chloride in this process, complex 3 then was treated with 2 equiv of Et₃NHCl. The product of this reaction was characterized in the solid state (Figure 1) after counteranion metathesis with NaBPh₄.

The orange-red cobalt nitrosyl complex 6 ($\nu_{\text{NO}} = 1636 \text{ cm}^{-1}$) was isolated by this procedure in 76% yield after crystallization. In accordance with other tetragonal {CoNO}⁸ species,²¹ complex 6 features a bent nitrosyl (Co–N–O = 122°) with a N–O bond length near that of free nitric oxide. The *trans*-coordinated chloride is at a long distance of 2.621 Å, consistent with the large *trans* influence that has been observed for bent nitrosyls.²² The water molecule that is formed upon protonation remains bound to the Mg center and is within hydrogen-bonding distance of the axial chloride.

Complex 6 exhibits an electrochemically reversible reduction (100 mV/s scan rate) at −0.65 V vs SCE. In attempts to generate the one-electron-reduced {CoNO}⁹ species using Cp₂Co as a chemical reductant, a new band in the IR spectrum (see the Supporting Information) was observed at 1691 cm^{−1} (¹⁵NO₂: 1656 cm^{−1}), tentatively assigned to a nitrosyl N–O stretching vibration. Further efforts to isolate this species and obtain additional characterization data have been precluded by its instability. Nevertheless, in situ generation of the reduced species as a solution in MeCN followed immediately by addition of Et₃NHCl produced free N₂O—detected by gas chromatographic analysis of the headspace volume—with no observable competing H₂ evolution.

Electrocatalytic Nitrite Reduction Activity. Overall, the series of stoichiometric reactions described above illustrate the ability of these CoMg bimetallic systems to coordinate NO₂[−] and mediate the successive addition of electrons and protons to the bound substrate, generating free N₂O as a terminal product. These results intimated the possibility of using complex 1 to carry out multiple turnovers of the overall 4e[−]/6H⁺ nitrite reduction process under electrocatalytic conditions. Transition-metal tetraazamacrocycles have been demonstrated to be competent multielectron reduction catalysts for a variety of small-molecule substrates, including NO₂[−]; however, achieving high selectivity for a single reduction product and minimizing competing H₂ evolution are persistent challenges.^{17,23}

Complex 1 exhibits two reversible redox couples at −0.32 and −1.03 V vs SCE. Both reduction events remain electrochemically reversible in the presence of 40 equiv of [*n*-Bu₄N][NO₂], but the potential for the first reduction wave is cathodically shifted by approximately 400 mV. Upon addition

of Et_3NHCl to this solution, the reductions become irreversible, and a current enhancement is observed, consistent with a catalytic process involving the consumption of multiple electron equivalents per catalyst molecule at the electrode surface. The onset potential is approximately 700 mV positive of that for the glassy carbon electrode alone.

To determine whether this multielectron process can be attributed to catalytic nitrite reduction, controlled-potential electrolysis experiments were conducted at -1.2 V vs SCE (Figure 7b). Over a 2 h period, 31 C of charge was passed,

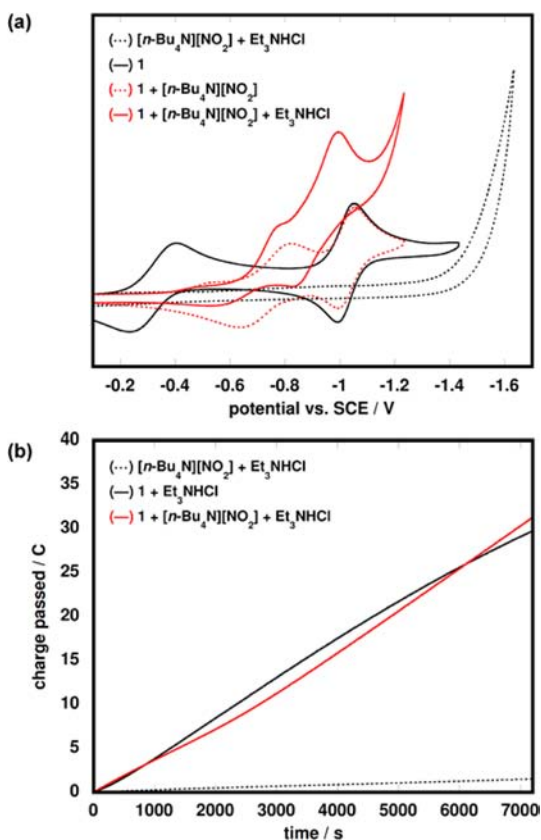


Figure 7. (a) Cyclic voltammograms for 0.5 mM complex **1** under various conditions (100 mV/s scan rate). (b) Cumulative charge passed during 2 h of bulk electrolyses (-1.2 V vs SCE) with 0.5 mM complex **1**. In CV and bulk electrolysis experiments, 20 mM concentrations of $[\text{n-Bu}_4\text{N}][\text{NO}_2]$ and Et_3NHCl were used (0.1 M $[\text{n-Bu}_4\text{N}][\text{ClO}_4]$ supporting electrolyte). The background activity of the glassy carbon electrode is shown for comparison.

corresponding to approximately 11 electron equivalents per catalyst. Analysis of the product mixture indicated the formation of gaseous N_2O with no detectable amounts of either NH_2OH or NH_3 in the solution phase. No competing evolution of H_2 was observed. Because the electrolyses were conducted under an atmosphere of N_2 , the formation of N_2 as a nitrite reduction product was not assessed. Under the same conditions, the glassy carbon electrode alone exhibited negligible background activity, passing only 1 C of charge over the 2 h period.

In the absence of NO_2^- , complex **1** reduces Et_3NHCl at -1.2 V vs SCE to produce H_2 with 96% faradic efficiency.^{15e,f} Similar amounts of charge are passed with and without NO_2^- . This result suggests that the strong association of nitrite with these complexes prevents competing protonation at the metal center

and suppresses the hydrogen evolution process that would otherwise occur at these potentials.

As a point of comparison, other cobalt and iron tetraazamacrocyclic complexes, which have been examined for electrocatalytic nitrite reduction in water, generally either are selective for NH_3 production or form mixtures of products that include N_2O , N_2 , NH_3 , and NH_2OH .^{17,23} Although the unusual selectivity for N_2O in this case may be a specific feature of complex **1**, the relative proton concentrations under aqueous and nonaqueous conditions likely also play a significant role.

Infrared spectroelectrochemical experiments²⁴ were performed to identify metal-containing species that are formed under electrolysis conditions (Figure 8). When a potential of

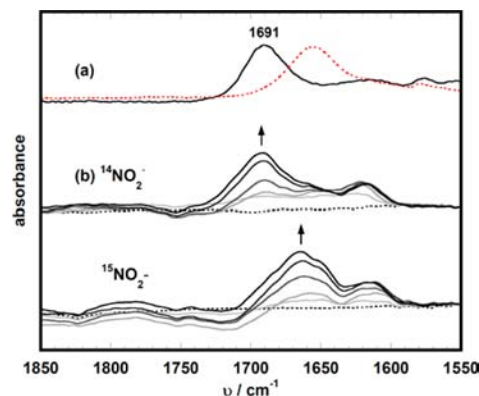


Figure 8. (a) ATR-IR spectra for the product mixture of the reduction of complex **6** with Cp_2Co . Spectra for material prepared from $^{14}\text{NO}_2^-$ (solid, black line) and $^{15}\text{NO}_2^-$ (dotted, red line) are shown. (b) Infrared spectroelectrochemical data highlighting IR bands that increase during the electrolysis of 5.0 mM complex **1**, 20 mM $[\text{n-Bu}_4\text{N}][\text{NO}_2]$, and 20 mM Et_3NHCl in MeCN at -1.2 V (0.1 M $[\text{n-Bu}_4\text{N}][\text{ClO}_4]$ supporting electrolyte, platinum working electrode). Spectra collected using $^{14}\text{NO}_2^-$ (top) and $^{15}\text{NO}_2^-$ (bottom) are shown.

-1.2 V was applied to a solution containing complex **1** in the presence of excess $[\text{n-Bu}_4\text{N}][\text{NO}_2]$ and Et_3NHCl , new prominent bands, sensitive to $^{15}\text{NO}_2^-$ isotopic labeling, were observed in the range of $1750\text{--}1600\text{ cm}^{-1}$, a characteristic N–O stretching frequency region for metal nitrosyl complexes. The position of the major band (1692 cm^{-1}) is identical within error to that of the product obtained from the stoichiometric, one-electron reduction of the nitrosyl complex **6**. These data are consistent with the intermediacy of a common $\{\text{CoNO}\}^9$ species in the N_2O evolution process under stoichiometric protonation conditions and during electrocatalysis.

On the basis of the collective data presented here, a plausible catalytic cycle is illustrated in Figure 9. Initial reduction of the $[(\mu\text{-OAc})(\text{Br})\text{CoMg}]^+$ precatalyst **1** by one electron followed by substitution of OAc^- with NO_2^- allows entry into the catalytic cycle and affords the cationic $[(\mu\text{-NO}_2)\text{CoMg}]^+$ complex **4**. Reduction of this intermediate to the neutral species **3** and protonation with 2 equiv of acid generates the cobalt nitrosyl **6**, which is capable of being reduced by another electron to form a putative $\{\text{CoNO}\}^9$ species. Protonation of this reduced nitrosyl complex leads to the presumed bimolecular elimination of N_2O (0.5 equiv per catalyst molecule). Association of the NO_2^- substrate with the resulting complex regenerates intermediate **4** and closes the catalytic cycle. While more detailed mechanistic studies under electro-

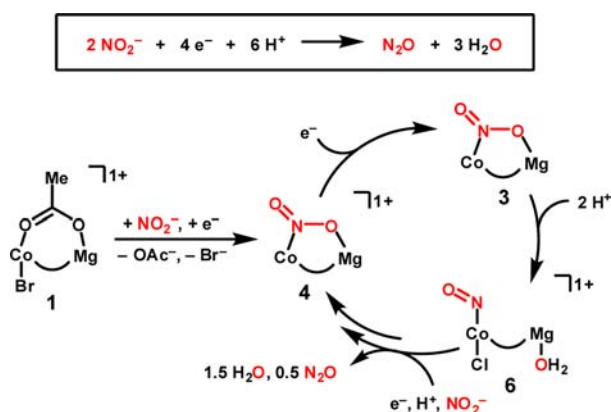


Figure 9. Proposed catalytic cycle for the $4e^-/6H^+$ reduction of 2 equiv of NO_2^- to form 1 equiv of N_2O using the precatalyst **1**.

catalytic conditions are warranted, this series of proposed intermediates is consistent with the stoichiometric reactivity of isolated and structurally characterized species.

CONCLUSIONS

In conclusion, the $\text{Co}(\text{doen})\text{Mg}$ heterobimetallic platform provides a potentially generalizable means of studying the role of secondary coordination sphere interactions in the activation of small molecules at a reduced metal center. In the specific case of nitrite reduction, the incorporation of a Mg^{2+} cation into the framework of a tetraazamacrocycle complex has allowed access to a previously uncharacterized nitrite adduct of $\text{Co}(\text{I})$. The activated N–O bond in this neutral $\mu\text{-NO}_2$ species undergoes heterolysis upon treatment with a mild acid. This process is accompanied by a significant expansion of the Co–Mg separation and a reorientation of the Me_3TACN ligand, demonstrating the geometric flexibility afforded by the diimine–dioxime scaffold. The resulting nitrosyl complex liberates N_2O upon successive treatment with 1 equiv of a reductant and an acid.

The accessibility of multiple conformations and oxidation states is an important feature of these complexes that allows a variety of intermediates to be stabilized in the course of a catalytic cycle. Accordingly, complex **1** has been found to be competent for the electrocatalytic conversion of NO_2^- to N_2O . Noteworthy features of the catalytic process include negligible competing hydrogen evolution and a high selectivity for the denitrification pathway over formation of NH_3 or NH_2OH . The application of these CoMg and related heterobimetallic complexes to other electrocatalytic reduction processes is an ongoing area of study.

EXPERIMENTAL SECTION

General Considerations. The preparation of **1** was conducted without protection from water or oxygen. All other manipulations were carried out using standard Schlenk or glovebox techniques under an atmosphere of dinitrogen. Solvents were dried and degassed by passage through a column of activated alumina and sparging with N_2 gas. Deuterated solvents were purchased from Cambridge Isotope Laboratories, Inc., degassed, and stored over activated 3 Å molecular sieves prior to use. Me_3TACN ²⁵ and $\text{Co}(\text{Me}^e\text{doenH})\text{Br}_2$ ²⁶ were prepared according to procedures reported in the literature. All other reagents and starting materials were purchased from commercial vendors and used without further purification unless otherwise noted. Elemental analyses were performed by Midwest Microlab (Indianapolis, IN).

Physical Methods. ^1H , ^{13}C , and ^{31}P NMR spectra were collected at room temperature on Varian 300 and 400 MHz NMR spectrometers. ^1H and ^{13}C NMR spectra are reported in parts per million relative to tetramethylsilane, using the residual solvent resonances as an internal standard. ^{31}P NMR spectra are reported in parts per million relative to 85% phosphoric acid. X-Band EPR spectra were recorded on a Bruker EMS spectrometer and simulated using the Easyspin program.²⁷ UV–vis measurements were acquired on a Cary 50 UV/vis spectrophotometer using a 1 cm two-window quartz cuvette. IR measurements were performed using a Bruker Alpha spectrometer equipped with a diamond ATR. Electrochemical measurements were performed using a CH Instruments 630-C electrochemistry analyzer. Cyclic voltammograms were acquired using a glassy carbon working electrode under an atmosphere of N_2 , and the potentials were internally referenced to the reversible Fc/Fc^+ couple (+0.38 V vs SCE).

X-ray Crystallography. Single-crystal X-ray diffraction studies were carried out at the Caltech Division of Chemistry and Chemical Engineering X-ray Crystallography Facility on a Bruker KAPPA APEX II or Bruker SMART 1000 diffractometer. Data were collected at 100 K using $\text{Mo K}\alpha$ radiation ($\lambda = 0.71073 \text{ \AA}$). Structures were solved by the direct or Patterson method using SHELXS and refined against F^2 on all data by full-matrix least-squares with SHELXL-97.²⁸

[(Br)($\mu\text{-OAc}$)Co(Me^edoen)Mg(Me_3TACN)]BPh₄ (1**).** A 215 mg sample of $\text{Mg}(\text{OAc})_2 \cdot 4\text{H}_2\text{O}$ (0.5 mmol, 1.0 equiv) was added as a solid to 171 mg of Me_3TACN (0.5 mmol, 1.0 equiv) in 10 mL of MeCN. The heterogeneous mixture was sonicated for 15 min. A 444 mg sample of $\text{Co}(\text{Me}^e\text{doenH})\text{Br}_2$ (0.5 mmol, 1.0 equiv) and 342 mg of NaBPh_4 (0.5 mmol, 1.0 equiv) were added successively. The reaction mixture was stirred at 50 °C for 12 h. After being cooled to room temperature, the mixture was filtered through a plug of Celite, and the filtrate was concentrated to a foam under reduced pressure. The residue was taken up in 2 mL of CH_2Cl_2 , and the mixture was allowed to stand at room temperature for 4 h, after which the mixture was filtered through a short plug of Celite. The filtrate was concentrated to dryness under reduced pressure. A 10 mL volume of MeOH was added, and the mixture was sonicated, causing a green-brown powder to separate. The solid material was collected on a fritted glass filter and washed with two 2 mL portions of MeOH and two 10 mL portions of Et_2O . The crude material was recrystallized by dissolving it in boiling MeOH (400 mL/1.0 g of crude material) containing Et_3NHBBr (100 mg/1.0 g of crude product), filtering the hot mixture to removed undissolved material, and allowing the mixture to cool to room temperature over a period of 12 h. The light brown crystals were collected on a glass frit, washed successively with two portions of 10 mL of MeOH and Et_2O , and dried under vacuum to yield 220 mg of **1** (0.24 mmol, 47% yield). Single crystals suitable for XRD were obtained according to this procedure. ^1H NMR (400 MHz, CD_3CN): $\delta = 7.37\text{--}7.21$ (m, 8 H), 7.07–6.93 (m, 8 H), 6.91–6.76 (m, 4 H), 4.64–4.36 (m, 4 H), 3.03–2.90 (m, 4 H), 2.88–2.73 (m, 4 H), 2.73–2.61 (m, 4 H), 2.65 (s, 3 H), 2.48 (s, 6 H), 2.41 (s, 6 H), 2.34 (s, 6 H), 1.58 (s, 3 H). $^{13}\text{C}\{^1\text{H}\}$ NMR (101 MHz, CD_3CN): $\delta = 183.1, 177.5, 165.2$ (q, $^1J_{\text{B-C}} = 49.6 \text{ Hz}$), 159.5, 137.2, 127.0, 123.2, 54.9, 54.2, 54.1, 54.0, 47.4, 47.3, 25.1, 18.7, 13.9. ESI-MS: m/z 618.0 (100), 616.1 (90) [(OAc)(Br)Co(Me^edoen)Mg(Me_3TACN)]⁺; 537.2 (10) [(OAc)Co(Me^edoen)Mg(Me_3TACN)]⁺. Anal. Calcd for **1** ($\text{C}_{45}\text{H}_{60}\text{BBrCoMgN}_7\text{O}_4$): C, 57.68; H, 6.45; N, 10.46. Found: C, 57.93; H, 6.56; N, 10.37.

[(PPh₃)Co(Me^edoen)Mg(Me_3TACN)(THF)]BPh₄ (2**).** A 46.8 mg sample of **1** (0.05 mmol, 1.0 equiv), 20.8 mg of Cp_2Co (0.11 mmol, 2.2 equiv), 15.7 mg of PPh_3 (0.06, 1.2 equiv), and 34.2 mg of NaBPh_4 (0.1 mmol, 2.0 equiv) were stirred in 2 mL of THF. Over the course of 30 min, a dark-blue-green-colored solution formed with precipitation of a colorless solid. An 8 mL sample of pentane was added, causing the product to precipitate. The mixture was filtered through a short plug of Celite, and the solid material was washed with one additional 5 mL portion of 4:1 pentane/THF and with pentane. The product was eluted through the Celite plug with three 2 mL portions of 1:1 pentane/THF. The filtrate was concentrated under reduced pressure to yield 40.2 mg of **2** as a dark teal-colored powder (0.035 mmol, 71%

yield). Single crystals suitable for X-ray diffraction were obtained by pentane vapor diffusion into a concentrated solution of **2** in THF. ^1H NMR (400 MHz, C_6D_6): δ = 7.05 (br s, 8 H), 7.15–6.99 (m, 9 H), 6.93 (t, J = 8.3 Hz, 6 H), 6.71 (br s, 8 H), 6.60 (br s, 4 H), 3.72–3.56 (m, 2 H), 3.11 (m, 2 H), 2.54–2.32 (m, 12 H), 2.23 (br s, 9 H), 1.75 (s, 6 H), 1.44 (s, 3 H), 1.41 (s, 3 H). $^{31}\text{P}\{^1\text{H}\}$ NMR (162 MHz, C_6D_6): δ = 43. UV-vis (C_6H_6): λ_{max} (nm) $\{\epsilon, \text{cm}^{-1} \text{M}^{-1}\}$ 617 {6000}. Anal. Calcd for **2** ($\text{C}_{65}\text{H}_{80}\text{BCoMgN}_7\text{O}_3\text{P}$): C, 68.94; H, 7.12; N, 8.66. Found: C, 67.97; H, 7.14; N, 8.13.

(μ -NO₂)Co(^{Me}doen)Mg(Me₃TACN) (3). A 187 mg sample of **1** (0.2 mmol, 1.0 equiv), 83.2 mg of Cp₂Co (0.44 mmol, 2.2 equiv), 57.7 mg of PPh₃ (0.22 mmol, 1.1 equiv), and 137 mg of NaBPh₄ (0.4 mmol, 2.0 equiv) were stirred in 4 mL THF for 1 h, producing a dark green solution and colorless precipitate. A 4 mL volume of pentane was added, and the reaction mixture was filtered through a plug of Celite, washing with four 1 mL portions of 1:1 pentane/THF. The filtrate was concentrated to a total volume of 2 mL. An 86.5 mg sample of [*n*-Bu₄N][NO₂] (0.3 mmol, 1.5 equiv) in 2 mL of THF was layered on top of the filtrate, and the sample and filtrate were allowed to mix over a period of 12 h. The darkly colored precipitate that formed was collected by filtration and washed successively with two 1 mL portions of THF and two 1 mL portions of Et₂O. After the precipitate was dried under vacuum, 83.5 mg of **3** (0.16 mmol, 80% yield) was obtained as darkly colored needles. Single crystals suitable for XRD were obtained in this manner. ^1H NMR (400 MHz, CD₃CN): δ = 4.30 (br s, 4 H), 2.75 (s, 3 H), 3.09–2.67 (m, 12 H), 2.61 (s, 6 H), 2.20 (s, 6 H), 2.13 (s, 6 H). UV-vis (C_6H_6): λ_{max} (nm) $\{\epsilon, \text{cm}^{-1} \text{M}^{-1}\}$ 700 {16,000}. ATR-IR (solid): $\nu(^{14}\text{NO}_2)$ = 1392, 1181 cm^{-1} ; $\nu(^{15}\text{NO}_2)$ = 1371, 1159 cm^{-1} . Anal. Calcd for **3**·0.33THF ($\text{C}_{20.33}\text{H}_{39.67}\text{CoMgN}_8\text{O}_{4.33}$): C, 44.50; H, 7.28; N, 20.42. Found: C, 44.30; H, 7.21; N, 20.30.

(μ -NO₂)Co(^{Me}doen)Mg(Me₃TACN)BPh₄ (4). A 15.7 mg sample of **3** (0.03 mmol, 1.0 equiv) and 12.6 mg of [Et₃NH][BPh₄] (0.03 mmol, 1.0 equiv) were stirred in 3 mL of THF for 24 h. The solution turned red-brown, and a darkly colored precipitate formed during this period. The reaction mixture was filtered through a short plug of Celite, and the solid material was washed with three 1 mL portions of THF. The product was eluted with four 1 mL portions of CH₂Cl₂. The filtrate was dried under vacuum to yield 19.2 mg of **4** (76% yield, 0.023 mmol) as a dark brown solid. Single crystals suitable for XRD were obtained by diffusion of pentane vapor into a 1:1 THF/CH₂Cl₂ solution at room temperature. UV-vis (MeCN): λ_{max} (nm) $\{\epsilon, \text{cm}^{-1} \text{M}^{-1}\}$ 418 {2600}. ATR-IR (solid): $\nu(^{14}\text{NO}_2)$ = 1437, 1190 cm^{-1} ; $\nu(^{15}\text{NO}_2)$ = 1410, 1171 cm^{-1} . Anal. Calcd for **4** ($\text{C}_{43}\text{H}_{57}\text{BCoMgN}_8\text{O}_4$): C, 61.19; H, 6.81; N, 13.28. Found: C, 60.95; H, 6.66; N, 13.07.

[(Br)(μ -NO₂)Co(^{Me}doen)Mg(Me₃TACN)]PF₆ (5). A 26.2 mg sample of **3** (0.05 mmol, 1.0 equiv), 33.1 mg of [Cp₂Fe][PF₆] (0.10 mmol, 2.0 equiv), and 16.1 mg of [*n*-Bu₄N][Br] (0.05 mmol, 1.0 equiv) were stirred in 5 mL of THF for 4 h, producing a pale orange-brown heterogeneous mixture. A 5 mL volume of pentane was added, and the mixture was filtered through a short plug of Celite. The product was eluted through the Celite plug with three 500 μL portions of MeCN. Diffusion of Et₂O vapor into the filtrate MeCN solution yielded 31.4 mg of orange crystals (0.034 mmol, 68% yield) that were suitable for XRD. ^1H NMR (400 MHz, CD₃CN): δ = 4.82–4.49 (m, 4 H), 2.86 (br s, 12 H), 2.43 (s, 6 H), 2.53–2.34 (m, 9 H), 2.28 (s, 6 H). $^{13}\text{C}\{^1\text{H}\}$ NMR (101 MHz, CD₃CN): δ = 178.6, 160.0, 55.4, 54.1, 46.9, 18.8, 13.9. ATR-IR (solid): $\nu(^{14}\text{NO}_2)$ = 1461, 1245 cm^{-1} ; $\nu(^{15}\text{NO}_2)$ = 1421, 1228 cm^{-1} . ESI-MS: m/z 604.8 (100), 602.9 (90) [(NO₂)(Br)-Co(^{Me}doen)Mg(Me₃TACN)]⁺; 524.1 (20) [(NO₂)Co(^{Me}doen)Mg-(Me₃TACN)]⁺. Anal. Calcd for **5** ($\text{C}_{19}\text{H}_{37}\text{BrCoFeMgN}_8\text{O}_4\text{P}$): C, 30.44; H, 4.97; N, 14.95. Found: C, 31.11; H, 4.91; N, 15.33.

[(Cl)(NO)Co(^{Me}doen)Mg(Me₃TACN)(H₂O)]BPh₄ (6). A 10.5 mg sample of **3** (0.02 mmol, 1.0 equiv) and 5.5 mg of Et₃NHCl (0.04 mmol, 2.0 equiv) were stirred in 1 mL of THF for 6 h. The reaction mixture remained heterogeneous throughout this period, and a red precipitate formed. A 6.8 mg sample of NaBPh₄ (0.02 mmol, 1.0 equiv) was added in 1 mL of THF, causing the red material to dissolve. The reaction mixture was filtered through a short plug of Celite. Diffusion of pentane vapor into the filtrate/THF solution at room

temperature yielded 13.3 mg of a red crystalline solid (0.015 mmol, 76% yield). Single crystals obtained according to this procedure were suitable for XRD. ^1H NMR (400 MHz, CD₃CN): δ = 7.34–7.17 (m, 8 H), 6.99 (m, 8 H), 6.84 (m, 4 H), 3.80 (s, 4 H), 2.83–2.50 (m, 12 H), 2.71 (m, 9 H), 2.36 (s, 6 H), 2.26 (s, 6 H). ATR-IR (solid): $\nu(^{14}\text{NO})$ = 1636 cm^{-1} ; $\nu(^{15}\text{NO})$ = 1604 cm^{-1} ; $\nu(\text{O-H})$ = 3205, 3345 cm^{-1} . Anal. Calcd for **6** ($\text{C}_{43}\text{H}_{59}\text{ClCoMgN}_8\text{O}_4$): C, 58.59; H, 6.75; N, 12.71. Found: C, 58.63; H, 7.06; N, 12.65.

(μ -OAc)Co(^{Me}doen)Mg(Me₃TACN)]BPh₄ (8). A 46.8 mg sample of **1** (0.05 mmol, 1.0 equiv) and 20.8 mg of Cp₂Co (0.11 mmol, 2.2 equiv) were stirred in 2 mL of THF. Over the course of 30 min, the solution turned red and a colorless precipitate formed. The reaction mixture was concentrated to dryness under reduced pressure. The residue was washed with three 2 mL portions of C₆H₆, redissolved in 2 mL of THF, and filtered through a short plug of Celite, washing with two additional portions of 2 mL THF. The filtrate was concentrated to dryness under reduced pressure to yield 35.1 mg of a red solid (0.41 mmol, 82% yield). Single crystals suitable for XRD were obtained by diffusion of pentane vapor into a concentrated solution of **8** in THF. UV-vis (THF): λ_{max} (nm) $\{\epsilon, \text{cm}^{-1} \text{M}^{-1}\}$: 521 {1000}. Anal. Calcd for **8**·THF ($\text{C}_{49}\text{H}_{68}\text{BCoMgN}_7\text{O}_5$): C, 63.34; H, 7.38; N, 10.55. Found: C, 63.46; H, 6.89; N, 10.34.

Stoichiometric Reduction and Protonation of 6. A 17.6 mg sample of **6** (0.02 mmol, 1.0 equiv) was dissolved in 2 mL of MeCN in a 50 mL Schlenk tube. A 4.5 mg sample of Cp₂Co (0.024 mmol, 1.2 equiv) was added as a suspension in 1 mL of MeCN. The mixture was stirred at room temperature for 15 min, during which time the solution darkened to a green-brown color. A solution of 3.3 mg of Et₃NHCl (0.024 mmol, 1.2 equiv) in 1 mL of MeCN was added by syringe through a septum, and the mixture was stirred in the sealed reaction vessel. After 30 min, the headspace was sampled using a gastight syringe, and the mixture was analyzed for H₂ and N₂O by GC.

Bulk Electrolysis Experiments. Controlled-potential electrolysis experiments were conducted in a sealed two-chambered H cell equipped with a glassy carbon plate working electrode (12 cm × 3 cm × 1 cm) and a silver reference electrode in the first chamber and a glassy carbon plate counter electrode in the second. The two chambers were separated by a fine-porosity glass frit. Prior to the start of each experiment, the solutions were sparged with N₂, and the cell was sealed under a N₂ atmosphere.

Electrolyses were performed in MeCN containing 0.1 M [*n*-Bu₄N][ClO₄] as a supporting electrolyte. In a typical procedure, the working-electrode chamber contained 0.5 mM complex **1**, 20 mM Et₃NHCl, and 20 mM [*n*-Bu₄N][NO₂]. Following the 2 h electrolysis period, gas-phase products (N₂O and H₂) were detected by sampling the headspace volume and analyzing the mixture by gas chromatography (Agilent 7890A gas chromatograph, HP-PLOT U and HP-PLOT Molesieve columns) using a thermal conductivity detector. To assess the presence of solution-phase products, 1 mL of 1.0 M HCl in Et₂O was added to the postelectrolysis mixture to protonate any NH₂OH or NH₃ that may have been formed. The solution was concentrated to dryness under reduced pressure, and the residue was partitioned between CH₂Cl₂ and H₂O. Selective chemical tests for NH₂OH²⁹ or NH₃³⁰ were performed on the aqueous phase.

Infrared Spectroelectrochemistry Experiments. The spectroelectrochemistry cell²⁴ (KBr window, platinum working electrode, silver pseudoreference electrode, and platinum counter electrode) was charged with a solution of 5.0 mM complex **1**, 20 mM [*n*-Bu₄N][NO₂], 20 mM Et₃NHCl, and 0.1 M [*n*-Bu₄N][ClO₄]. A background spectrum was acquired prior to the electrolysis and subtracted from subsequent spectra that were acquired. A potential of –1.2 V was applied, and spectra were collected every minute for a 5 min period. This procedure was repeated using $^{15}\text{NO}_2^-$.

■ ASSOCIATED CONTENT

Supporting Information

Experimental details, spectra, DFT calculations, XRD data, and CIF data. This material is available free of charge via the Internet at <http://pubs.acs.org>.

■ AUTHOR INFORMATION

Corresponding Author

jpeters@caltech.edu

Notes

The authors declare no competing financial interest.

■ ACKNOWLEDGMENTS

This work was supported by the National Science Foundation Center for Chemical Innovation on Solar Fuels (CCI Solar, Grant CHE-0802907) and the Gordon and Betty Moore Foundation. We thank Larry M. Henling for assistance with crystallography, Angelo Di Bilio for assistance with EPR measurements, and David Lacy for assistance with IR spectroelectrochemical experiments.

■ REFERENCES

- (1) (a) Toth, J. E.; Anson, F. C. *J. Am. Chem. Soc.* **1989**, *111*, 2444–2451. (b) Rhodes, M. R.; Barley, M. H.; Meyer, T. J. *Inorg. Chem.* **1991**, *30*, 629–635. (c) Brylev, O.; Sarrazin, M.; Roué, L.; Bélanger, D. *Electrochim. Acta* **2007**, *52*, 6237–6247. (d) Coleman, D. H.; White, R. E.; Hobbs, D. T. *J. Electrochem. Soc.* **1995**, *142*, 1152–1161.
- (2) Smieja, J. M.; Benson, E. E.; Kumar, B.; Grice, K. A.; Seu, C. S.; Miller, A. J. M.; Mayer, J. M.; Kubiak, C. P. *Proc. Natl. Acad. Sci. U.S.A.* **2012**, *109*, 15646–15650.
- (3) Eady, R. R. *Chem. Rev.* **1996**, *96*, 3013–3030.
- (4) For discussions of secondary coordination sphere interactions in CO₂ reduction, see: (a) Benson, E. E.; Kubiak, C. P.; Sathrum, A. J.; Smieja, J. M. *Chem. Soc. Rev.* **2009**, *38*, 89–99. (b) Dubois, M. R.; Dubois, D. L. *Acc. Chem. Res.* **2009**, *42*, 1974–1982. (c) Jeoung, J.-H.; Dobbek, H. *Science* **2007**, *318*, 1461–1464. (d) Krogman, J. P.; Foxman, B. M.; Thomas, C. M. *J. Am. Chem. Soc.* **2011**, *133*, 14582–14585. (e) Costentin, C.; Drouet, S.; Robert, M.; Savéant, J.-M. *Science* **2012**, *338*, 90–94.
- (5) (a) Williams, P. A.; Fulop, V.; Garman, E. F.; Saunders, N. F. W.; Ferguson, S. J.; Hajdu, J. *Nature* **1997**, *389*, 406–412. (b) Ranghino, G.; Scorza, E.; Sjögren, T.; Williams, P. A.; Ricci, M.; Hajdu, J. *Biochemistry* **2000**, *39*, 10958–10966.
- (6) For discussions of the effect of hydrogen bonding on nitrite binding to myoglobin, see: (a) Xu, N.; Yi, J.; Richter-Addo, G. B. *Inorg. Chem.* **2010**, *49*, 6253–6266. (b) Zahran, Z. N.; Chooback, L.; Copeland, D. M.; West, A. H.; Richter-Addo, G. B. *J. Inorg. Biochem.* **2008**, *102*, 216–233. (c) Yi, J.; Heinecke, J.; Tan, H.; Ford, P. C.; Richter-Addo, G. B. *J. Am. Chem. Soc.* **2009**, *131*, 18119–18128.
- (7) Cutruzzolà, F.; Brown, K.; Wilson, E. K.; Bellelli, A.; Arese, M.; Tegoni, M.; Cambillau, C.; Brunori, M. *Proc. Natl. Acad. Sci. U.S.A.* **2001**, *98*, 2232–2237.
- (8) Einsle, O.; Messerschmidt, A.; Huber, R.; Kroneck, P. M. H.; Neese, F. *J. Am. Chem. Soc.* **2002**, *124*, 11737–11745.
- (9) For discussions of biologically relevant nitrite reduction at cobalt, see: (a) Fujita, E.; Chang, C. K.; Fajer, J. *J. Am. Chem. Soc.* **1985**, *107*, 7665–7669. (b) Heinecke, J. L.; Yi, J.; Pereira, J. C. M.; Richter-Addo, G. B.; Ford, P. C. *J. Inorg. Biochem.* **2012**, *107*, 47–53.
- (10) (a) Yeh, C.-Y.; Chang, C. J.; Nocera, D. G. *J. Am. Chem. Soc.* **2001**, *123*, 1513–1514. (b) Chang, C. J.; Chng, L. L.; Nocera, D. G. *J. Am. Chem. Soc.* **2003**, *125*, 1866–1876. (c) Shirin, Z.; Hammes, B. S.; Young, V. G.; Borovik, A. S. *J. Am. Chem. Soc.* **2000**, *122*, 1836–1837. (d) MacBeth, C. E.; Golombek, A. P.; Young, V. G.; Yang, C.; Kuczera, K.; Hendrich, M. P.; Borovik, A. S. *Science* **2000**, *289*, 938–941. (e) Borovik, A. S. *Acc. Chem. Res.* **2005**, *38*, 54–61. (f) Shook, R. L.; Borovik, A. S. *Inorg. Chem.* **2010**, *49*, 3646–3660.
- (11) (a) Fachinetti, G.; Floriani, C.; Zanazzi, P. F. *J. Am. Chem. Soc.* **1978**, *100*, 7405–7407. (b) Gambarotta, S.; Arena, F.; Floriani, C.; Zanazzi, P. F. *J. Am. Chem. Soc.* **1982**, *104*, 5082–5092. (c) Kanady, J. S.; Tsui, E. Y.; Day, M. W.; Agapie, T. *Science* **2011**, *333*, 733–736. (d) Park, Y. J.; Ziller, J. W.; Borovik, A. S. *J. Am. Chem. Soc.* **2011**, *133*, 9258–9261. (e) Lacy, D. C.; Park, Y. J.; Ziller, J. W.; Yano, J.; Borovik, A. S. *J. Am. Chem. Soc.* **2012**, *134*, 17526–17535.
- (12) Uyeda, C.; Peters, J. C. *Chem. Sci.* **2013**, *4*, 157–163.
- (13) (a) Luneau, D.; Oshio, H.; Okawa, H.; Kida, S. *J. Chem. Soc., Dalton Trans.* **1990**, 2283–2286. (b) Luneau, D.; Oshio, H.; Okawa, H.; Koikawa, M.; Kida, S. *Bull. Chem. Soc. Jpn.* **1990**, *63*, 2212–2217. (c) Birkelbach, F.; Winter, M.; Floerke, U.; Haupt, H.-J.; Butzlaff, C.; Lengen, M.; Bill, E.; Trautwein, A. X.; Wiegardt, K.; Chaudhuri, P. *Inorg. Chem.* **1994**, *33*, 3990–4001. (d) Ruiz, R.; Lloret, F.; Julve, M.; Carmen Muñoz, M.; Bois, C. *Inorg. Chim. Acta* **1994**, *219*, 179–186. (e) Cervera, B.; Ruiz, R.; Lloret, F.; Julve, M.; Faus, J.; Muñoz, M. C.; Journaux, Y. *Inorg. Chim. Acta* **1999**, *288*, 57–68. (f) Kiani, S.; Staples, R. J.; Ted Treves, S.; Packard, A. B. *Polyhedron* **2009**, *28*, 775–781.
- (14) For related trimetallic complexes of glyoximate ligands, see: (a) Okawa, H.; Koikawa, M.; Kida, S.; Luneau, D.; Oshio, H. *J. Chem. Soc., Dalton Trans.* **1990**, 0, 469–475. (b) Chaudhuri, P.; Winter, M.; Della Vedova, B. P. C.; Bill, E.; Trautwein, A.; Gehring, S.; Fleischhauer, P.; Nuber, B.; Weiss, J. *Inorg. Chem.* **1991**, *30*, 2148–2157. (c) Li, C. H.; Wang, R.-J.; Kou, H.-Z.; Li, Y. *Acta Crystallogr., Sect. E* **2003**, *59*, m608–m610. (d) Kobayashi, Y.; Ueki, S.; Ishida, T.; Nogami, T. *Chem. Phys. Lett.* **2003**, *378*, 337–342. (e) Ueki, S.; Ishida, T.; Nogami, T.; Choi, K.-Y.; Nojiri, H. *Chem. Phys. Lett.* **2007**, *440*, 263–267. (f) Fujiwara, K.; Okazawa, A.; Kojima, N.; Tanaka, G.; Yoshii, S.; Nojiri, H.; Ishida, T. *Chem. Phys. Lett.* **2012**, *530*, 49–54. (g) Kelley, P.; Radlauer, M. R.; Yanez, A. J.; Day, M. W.; Agapie, T. *J. Chem. Soc., Dalton Trans.* **2012**, *41*, 8086–8092.
- (15) (a) Connolly, P.; Espenson, J. H. *Inorg. Chem.* **1986**, *25*, 2684–2688. (b) Hu, X.; Cossairt, B. M.; Brunshwig, B. S.; Lewis, N. S.; Peters, J. C. *Chem. Commun.* **2005**, 4723–4725. (c) Hu, X.; Brunshwig, B. S.; Peters, J. C. *J. Am. Chem. Soc.* **2007**, *129*, 8988–8998. (d) Baffert, C.; Artero, V.; Fontecave, M. *Inorg. Chem.* **2007**, *46*, 1817–1824. (e) Jacques, P.-A.; Artero, V.; Pecaut, J.; Fontecave, M. *Proc. Natl. Acad. Sci. U.S.A.* **2009**, *106*, 20627–20632. (f) McCrory, C. C. L.; Uyeda, C.; Peters, J. C. *J. Am. Chem. Soc.* **2012**, *134*, 3164–3170.
- (16) (a) Hörold, S.; Vorlop, K. D.; Tacke, T.; Sell, M. *Catal. Today* **1993**, *17*, 21–30. (b) Pintar, A.; Batista, J.; Levec, J. *Catal. Today* **2001**, *66*, 503–510.
- (17) (a) Taniguchi, I.; Nakashima, N.; Matsushita, K.; Yasukouchi, K. *J. Electroanal. Chem. Interfacial Electrochem.* **1987**, *224*, 199–209. (b) Cheng, S.-H.; Su, Y. O. *Inorg. Chem.* **1994**, *33*, 5847–5854. (c) Kudrik, E. V.; Makarov, S. V.; Zahl, A.; van Eldik, R. *Inorg. Chem.* **2003**, *42*, 618–624.
- (18) (a) Pezeshk, A.; Greenaway, F. T.; Dabrowiak, J. C.; Vincow, G. *Inorg. Chem.* **1978**, *17*, 1717–1725. (b) Pezeshk, A.; Greenaway, F. T.; Vincow, G. *Inorg. Chem.* **1978**, *17*, 3421–3425.
- (19) The Mulliken spin population at Co, calculated at the B3LYP/6-31G(d) level of DFT, decreases from 1.03 for [(μ-OAc)CoMg]⁺ to 0.96 for [(μ-NO₂)CoMg]⁺.
- (20) For a review and selected examples of redox-active ligands containing an imine, see: (a) Lyaskovskyy, V.; de Bruin, B. *ACS Catal.* **2012**, *2*, 270–279. (b) Bart, S. C.; Chlopek, K.; Bill, E.; Bouwkamp, M. W.; Lobkovsky, E.; Neese, F.; Wiegardt, K.; Chirik, P. J. *J. Am. Chem. Soc.* **2006**, *128*, 13901–13912. (c) Hess, C. R.; Weyhermüller, T.; Bill, E.; Wiegardt, K. *Angew. Chem., Int. Ed.* **2009**, *48*, 3703–3706. (d) Myers, T. W.; Kazem, N.; Stoll, S.; Britt, R. D.; Shanmugam, M.; Berben, L. A. *J. Am. Chem. Soc.* **2011**, *133*, 8662–8672.
- (21) For selected examples, see: (a) Feltham, R. D.; Nyholm, R. S. *Inorg. Chem.* **1965**, *4*, 1334–1339. (b) Weaver, D. L.; Snyder, D. A. *Inorg. Chem.* **1970**, *9*, 2760–2767. (c) Scheidt, W. R.; Hord, J. L. *J. Am. Chem. Soc.* **1973**, *95*, 8281–8288. (d) Haller, K. J.; Enemark, J. H. *Acta Crystallogr., Sect. B* **1978**, *34*, 102–109. (e) Franz, K. J.; Doerrler, L. H.; Spingler, B.; Lippard, S. J. *Inorg. Chem.* **2001**, *40*, 3774–3780.
- (22) (a) Pratt, C. S.; Coyle, B. A.; Ibers, J. A. *J. Chem. Soc. A* **1971**, 0, 2146–2151. (b) Noell, J. O.; Morokuma, K. *Inorg. Chem.* **1979**, *18*, 2774–2782.
- (23) (a) Barley, M. H.; Meyer, T. J. *J. Am. Chem. Soc.* **1986**, *108*, 5876–5885. (b) Barley, M. H.; Rhodes, M. R.; Meyer, T. J. *Inorg. Chem.* **1987**, *26*, 1746–1750. (c) Younathan, J. N.; Wood, K. S.; Meyer, T. J. *Inorg. Chem.* **1992**, *31*, 3280–3285.
- (24) Zavarine, I. S.; Kubiak, C. P. *J. Electroanal. Chem.* **2001**, *495*, 106–109.

- (25) Niibayashi, S.; Hayakawa, H.; Jin, R.-H.; Nagashima, H. *Chem. Commun.* **2007**, 1855–1857.
- (26) (a) Uhlig, E.; Friedrich, M. Z. *Anorg. Allg. Chem.* **1966**, 343, 299–307. (b) Costa, G.; Mestroni, G.; de Savorgnani, E. *Inorg. Chim. Acta* **1969**, 3, 323–328. (c) Kitiphaisalnont, P.; Thohinung, S.; Hanmungtum, P.; Chaichit, N.; Patrakorn, S.; Siripaisarnpipat, S. *Polyhedron* **2006**, 25, 2710–2716.
- (27) Stoll, S.; Schweiger, A. J. *Magn. Reson.* **2006**, 178, 42–55.
- (28) Sheldrick, G. *Acta Crystallogr., Sect. A* **2008**, 64, 112–122.
- (29) Frear, D. S.; Burrell, R. C. *Anal. Chem.* **1955**, 27, 1664–1665.
- (30) Weatherburn, M. W. *Anal. Chem.* **1967**, 39, 971–974.